5. THE ATMOSPHERIC ENVIRONMENT OBSERVED AT BIG BEND NATIONAL PARK DURING THE BRAVO STUDY

The BRAVO Study intensively researched the properties of the particulate matter, atmospheric optics, meteorology, and air pollutant emissions of the study area during July through October 1999. The study also explored transport and diffusion by injecting perfluorocarbon tracers into the atmosphere at specific locations. Findings produced by these multiple experiments concerning the environment around Big Bend National Park and throughout the study area are summarized in this chapter. Some of these findings were carried into the source attribution analyses that are described in Chapters 10 and 11, while others advanced scientific understanding for future application. More detail on many of these studies and their results is provided in published papers and reports that are cited in the text; some of the reports are in the Appendix.

5.1 Particulate Matter Characterization by the Routine Measurement Network

As described in Section 3.3, the BRAVO Study included an extensive network of particulate matter samplers that routinely collected 24-hour and 6-hour samples over the four-month study period. This section summarizes findings derived from the routine measurements concerning the temporal and spatial characteristics of the study area particulate matter and its composition.

5.1.1 Particulate Matter Temporal and Spatial Characteristics

Evaluation of BRAVO Study particulate matter sample composition and temporal variation found similar behavior at groups of adjacent sampling sites in the study domain. The map in Figure 5-1 shows the grouping of sampling sites that this evaluation suggested. To provide a manageable description of the study period aerosol, concentration measurements at sites within each group were averaged together.

Figure 5-2 shows the time series of daily values of $PM_{2.5}$ sulfate and SO_2 at the K-Bar site in Big Bend National Park. The figure also shows the fraction of the total sulfur that is accounted for by sulfate. Six major sulfate episodes and four SO_2 episodes are evident in this figure. The episodes of elevated SO_2 concentrations were always associated with high sulfate concentrations; sulfates typically accounted for 75 to 85% of the total sulfur during those episodes. A common pattern among the sulfur episodes is a rise in sulfate after passages of cold fronts or stationary fronts in Texas, when the easterly wind component was often enhanced. Humidity-induced particle growth was substantial during the mid-September episode, but was not very significant for the other episodes (humidity-caused enhancement of light scattering, f(RH), was generally by a factor of 1.5 or less). Note, though, that while RH was not usually high at Big Bend, humidity was typically high in eastern Texas. The high humidity may have enhanced SO_2-to-sulfate (gas to particle) conversion prior to transport to Big Bend.

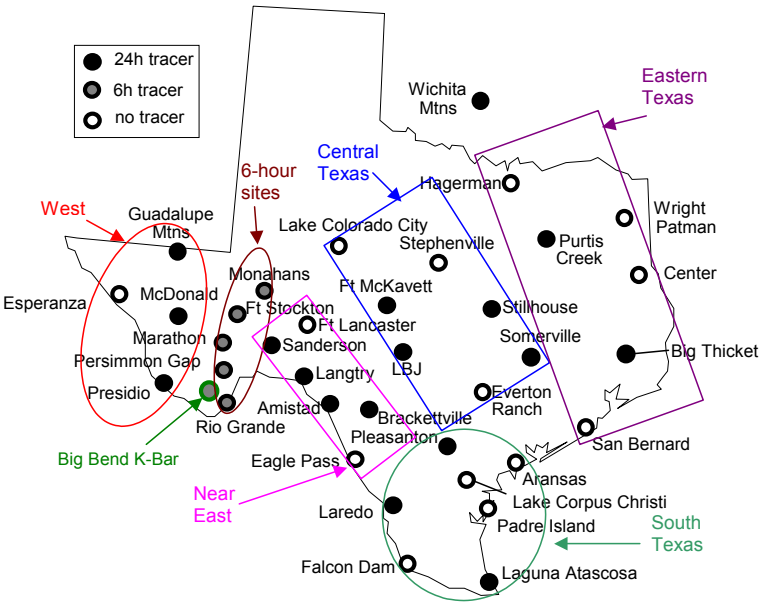

Figure 5-1. *Groups of BRAVO sampling sites that showed similar particulate matter behavior.*

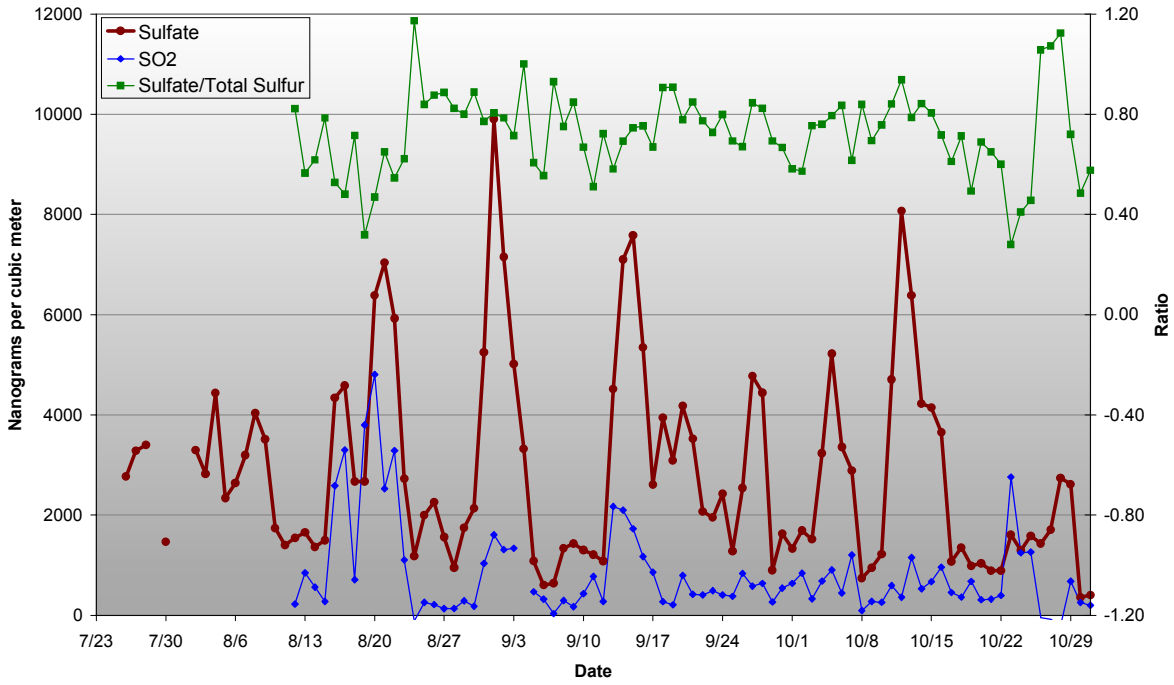

Figure 5-2. *Sulfate and SO_2 time series at K-Bar (left scale) and sulfate as fraction of total sulfur (right scale).*

Sulfate was closely associated with ammonium, and was present as a mixture of ammonium sulfate and ammonium bisulfate, i.e., ammonium to sulfate ion equivalent ratios varied between 0.5 and 1 (i.e., molar ratios ranged from 1 to 2). Excluding one outlier, the mean ammonium to sulfate ion equivalent ratio was 0.8 ± 0.2, and the aerosol was never

fully neutralized. The ratio did not change during sulfate episodes, but it did increase slightly from an average of 0.7 ± 0.1 before mid-September to 0.9 ± 0.1 from mid-September to the end of the study. A ratio of 1.0 indicates fully neutralized sulfate.

The nitrate ion concentration was at least a factor of ten lower than that of sulfate, and was not associated with ammonium. During some periods, it was highly correlated with sodium, though.

The early part of the study was characterized by several episodes of elevated fine soil concentrations. During these periods, the Fe/Ca ratio was also elevated and 5-day back trajectories frequently indicated rapid transport from the Caribbean, suggesting the possible influence of Saharan dust. (The influence of Saharan dust is covered in more detail in Sections 5.4 and 10.3.)

As an example, we will discuss the August 29-September 4 sulfur episode, which had the highest sulfur concentration during the BRAVO Study. A few days earlier (August 27) widespread haze was reported throughout a large area of the eastern United States. High sulfate concentrations first appeared in northeastern Texas and then spread across the state to Big Bend by September 1. Haze was reported on September 1, with visibility of just a few miles at many National Weather Service stations in central and southern Texas (Del Rio, Laredo, San Antonio, Harlingen, and Corpus Christi).

Figure 5-3 shows the fine particulate matter composition across Texas during this period. Note the high sulfate and organic mass in eastern Texas, and even at Wichita Mountains, Oklahoma, decreasing across the state to Big Bend. Concentrations in the southern part of the state were lower than elsewhere during this period.

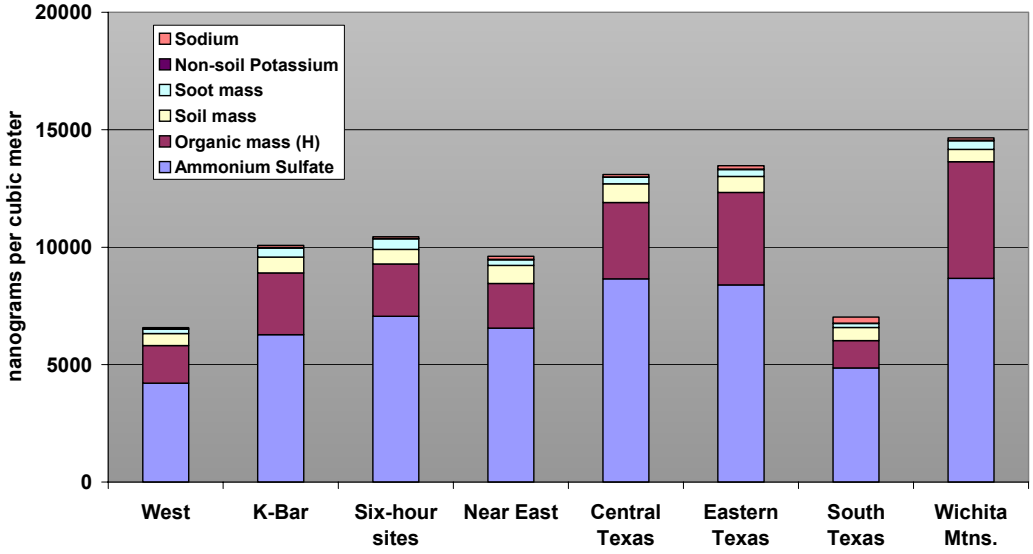

Figure 5-3. *Composition of $PM_{2.5}$ aerosol throughout Texas during the August 29-September 4, 1999, sulfate episode at Big Bend. Organic mass (H) refers to organic matter concentrations inferred from hydrogen atom measurements. All of the particulate sulfur is assumed to be in the form of ammonium sulfate, whose concentration is thus 4.125 times the measured elemental sulfur concentration.*

As was the case with all sulfur episodes, the passage of weather fronts preceded this episode. On August 29-31 a cold front oriented east-west was driven southward and even slightly westward by the clockwise circulation around a high pressure system centered in Manitoba. This "back-door" cold front would be conducive to transport of air from the Ohio River Valley into Texas. (The meteorology of this episode is discussed further in Section 5.4.)

Later episodes, starting in mid-September, had flow from the southeast as the front approached, followed by light northeasterly and easterly flow after passage. Little if any transport from the Ohio River Valley would be expected under these conditions, but transport from eastern Texas and nearby areas would be expected. Back-trajectory analyses and dispersion modeling support these conclusions, as shown later in this report.

Thus some episodes at Big Bend seemed to be related to emissions from within Texas, while others were affected by sources farther to the east or to the south. The large-scale meteorology suggests that air quality at Big Bend may be affected by sources in the eastern and midwestern United States during some periods.

Further insight into the spatial and temporal patterns of the particulate matter concentrations is provided by the animations that are described in Section 8.6 and are included in the Appendix. Additional discussion of study period meteorology appears in Section 5.4.

5.1.2 Properties of Particulate Matter at Big Bend National Park

The IMPROVE sampling system was used at the K-Bar site in Big Bend National Park to collect samples of particulate matter with aerodynamic diameters smaller than 2.5 and 10 μm ($PM_{2.5}$ and PM_{10}, respectively). Samples were analyzed to determine concentrations of elements, ions, carbonaceous material, and gravimetric mass less than 2.5 and 10.0 μm. The filter samples were collected each day starting at 8:00 a.m. In addition, size resolved particle measurements were made using an 8-stage Micro Orifice Uniform Deposit Impactor (MOUDI) sampling system that covered the same size range, and substrates were analyzed for inorganic species, including sulfate, nitrate, and ammonium ions.

The findings from the measurements of the IMPROVE and MOUDI samplers were combined to develop a complete description of the ambient particulate matter. The data analyses that were carried out are described in detail in the CIRA/NPS report on the BRAVO Study (Schichtel et al., 2004), which is included in the Appendix. We summarize here the procedures that were followed and the key findings.

The fine PM species at most continental sites can be classified into five major types: sulfates, nitrates, organics, light-absorbing carbon (LAC), and soil. Other fine species such as non-soil potassium, sea salt, and other trace elements are less important from a visibility standpoint there. Most fine sulfates are the result of oxidation of SO_2 gas to sulfate particles.

The masses of the various components of particulate matter were calculated using procedures described by Malm et al. (1994). Ammoniated sulfate[1] mass was calculated as $0.944[NH_4]+1.02[SO_4]$ (a formula that accounts for the mass of the hydrogen atom present in some forms of ammoniated sulfate and thus works for all degrees of neutralization). Organic carbon mass concentration (OCM) was estimated as 1.4[OC], where the factor of 1.4 approximately adjusts the organic carbon mass for other elements associated with the carbon molecule. Assuming that the collected nitrate ion is associated with fully neutralized sodium nitrate particles ($NaNO_3$), the nitrate compound mass was estimated from the nitrate ion mass concentration by multiplying by 1.37.

Soil mass concentration was estimated by summing the elements predominantly associated with soil, plus oxygen for the common compounds (Al_2O_3, SiO_2, CaO, K_2O, FeO, Fe_2O_3, TiO_2), plus a correction based on published data for other compounds such as MgO, Na_2O, water, and carbonate.

The sum of the five constituents and water provide a reasonable estimate of the fine mass measured gravimetrically on the Teflon filter, except that a significant fraction of the nitrate particulate mass could volatilize from the Teflon filter during collection and would not measured by gravimetric analysis. The nitrate artifact was not important here, where nitrate accounted for a very small percentage of the fine mass and sodium nitrate is presumably less volatile than ammonium nitrate.

Fine mass component concentrations at Big Bend are summarized in Table 5-1. Measured fine mass is about 8% greater than the fine mass reconstructed from the sum of the component masses. Ammoniated sulfate contributed 50% of the mass and organics and soil contributed 21% and 23%, respectively.

Table 5-1. Summary of fine mass component concentrations (in $\mu g/m^3$) at Big Bend National Park. The fraction that each component contributes to reconstructed fine mass is in parentheses.

Component	Mean	Std Dev.	Minimum	Maximum
Fine Mass (FM)	6.85	4.33	0.04	19.22
Reconstructed FM	6.36	3.42	1.05	16.89
Ammoniated sulfate	3.15 (50%)	2.19	0.41	10.66
Sulfate ion	2.48	1.79	0.30	8.57
$NaNO_3$	0.23 (4%)	0.14	0.02	0.93
Nitrate ion	0.17	0.10	0.02	0.68
OCM	1.34 (21%)	0.78	0.13	5.10
LAC	0.15 (2%)	0.10	0.00	0.52
SOIL	1.45 (23%)	1.74	0.03	8.63

[1] Ammoniated sulfate is defined as sulfate ions combined with any number of ammonium ions. Examples of ammoniated sulfate include (partially neutralized) ammonium bisulfate, NH_4HSO_4, with one ammonium ion, and letovicite, $(NH_4)_3H(SO_4)_2$, with 1.5 ammonium ions per sulfate ion; and (fully neutralized) ammonium sulfate, $(NH_4)_2SO_4$, with 2 ammonium ions.

On the other hand, as shown in Table 5-2, reconstructed coarse mass is 16% greater than gravimetric mass. Coarse mass (here PM_{10}-$PM_{2.5}$) has usually been interpreted as crustal material; although Table 5-2 shows that 31% of reconstructed coarse mass was carbon-based material, while soil or crustal material made up 53% of reconstructed coarse mass. Nitrates were interpreted as sodium nitrate because MOUDI mass size distribution measurements showed very little ammonium in the coarse mode and very little sodium in the fine mode. Coarse nitrate contributed 8% of the coarse mass.

Table 5-2. Summary of coarse mass concentrations (in $\mu g/m^3$) at Big Bend National Park.

Variable	Mean	Std Dev	Minimum	Maximum
Coarse Mass (CM)	4.69	4.31	0.00	29.01
Reconstructed CM	5.42	4.54	0.00	32.02
Ammoniated sulfate	0.45 (8%)	0.68	0.00	3.59
Sulfate ion	0.36	0.52	0.00	2.76
$NaNO_3$	0.41 (8%)	0.35	0.00	1.81
Nitrate ion	0.30	0.26	0.00	1.32
OCM	1.58 (29%)	1.13	0.00	7.14
LAC	0.09 (2%)	0.09	0.00	0.31
SOIL	2.90 (53%)	3.27	0.00	23.66

5.2 Detailed Characterization of the Particulate Matter at Big Bend National Park

In addition to routine measurements with IMPROVE samplers during the entire four months, specialized particulate matter measurements took place at the K-Bar site in Big Bend National Park, either during the full duration of the study or for a portion of it. The principal results of these measurements are presented in this section.

Results of the following special studies are summarized here

- Ionic composition of particulate matter;
- Concentrations of sulfates at 12-minute intervals;
- Identifying tracers of sources of organic particles;
- Size distributions of dried particles; and
- Very fine particulate matter measurements to identify sources of particulate matter.

5.2.1 Ionic Composition of Big Bend Particulate Matter

The chemical compositions of $PM_{2.5}$ and size-resolved particles were measured from July to October 1999 at the K-Bar site in Big Bend National Park. Daily $PM_{2.5}$ samples were collected using a University Research Glassware (URG) cyclone/annular denuder/filter pack sampling system consisting of a $PM_{2.5}$ cyclone inlet, two coated annular denuders in series (for nitric acid and ammonia), and a filter pack containing Teflon and nylon filters in series. Filters and denuders were extracted and analyzed on-site to minimize potential artifacts associated with sample storage. A Micro Orifice Uniform Deposit Impactor (MOUDI) was used to collect 24 hr size-resolved aerosol particle samples in 9 size categories (D_{50} = 18, 10, 5.6, 3.2, 1.8, 1.0, 0.56, 0.32 and 0.18 μm). MOUDI samples were archived and 41 sample days were selected for later analysis of the ionic chemical composition as a function of particle size. MOUDI samples were selected for analysis based on interesting $PM_{2.5}$ composition measurement, e.g., high sulfate, high nitrate, and suspected sea salt days) and other BRAVO Study results (particle size distributions and thermodynamic modeling studies). $PM_{2.5}$ and size-resolved aerosol concentrations of Cl^-, SO_4^{2-}, NO_3^-, Na^+, NH_4^+, K^+, Mg^{2+}, and Ca^{2+} were obtained through ion chromatographic analysis of the filter and impactor samples. Aerosol acidity was also measured (on-site) in the daily $PM_{2.5}$ filter samples.

The composition of these samples of $PM_{2.5}$ was dominated by sulfate and ammonium. Daily average sulfate and ammonium concentrations were strongly correlated (R^2 = 0.94). The molar ratio of ammonium to sulfate averaged 1.54 with a standard deviation of 0.30, which compares well with the average molar ratio of 1.6 ± 0.4 (ion equivalent ratio of 0.8 ± 0.2) reported in Section 5.1.1 for BRAVO-study IMPROVE sampler measurements. This ratio is also consistent with direct pH measurements of aerosol acidity, as shown in Figure 5-4. The highest concentrations of sulfate were observed from August to October, reaching as high as 8.5 $\mu g/m^3$.

The size-dependent composition obtained from the MOUDI samples reveals that most of the particulate nitrate is associated with coarse mode particles (typical peak size range of ~ 4 to 5 μm aerodynamic diameter) while sulfate is found predominantly in submicron particles (typical mode size of 0.4-0.5 μm aerodynamic diameter). Measured $PM_{2.5}$ nitrate concentrations primarily reflected capture of the lower end of the coarse particle nitrate mode; a 1-μm (aerodynamic diameter) size cut would have provided a better division between the fine and coarse aerosol modes. Particle nitrate concentrations were correlated with the sum of aerosol Na^+ and Ca^{2+} concentrations (R^2 = 0.70 and 0.60 for MOUDI and URG samples, respectively), demonstrating the importance of sea salt and soil dust particles in providing non-acidic surfaces for the condensation of nitric acid. While total nitrate concentrations (the sum of gaseous nitric acid and particulate nitrate) were correlated with aerosol sulfate concentrations (R^2 = 0.55), particle nitrate concentrations showed poor correlation with sulfate (R^2 = 0.004). High particle nitrate concentrations occurred during periods of transport from the Gulf of Mexico and/or across arid regions including northern Mexico and north central Texas.

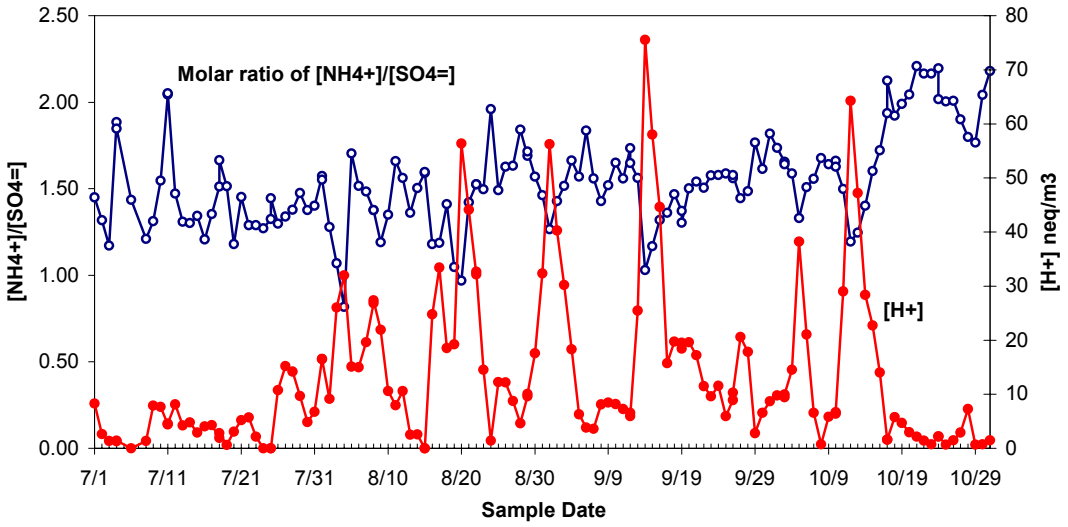

Figure 5-4. *Timelines of the $PM_{2.5}$ molar ratio of NH_4^+/SO_4^{2-} and aerosol acidity at Big Bend National Park.*

Thermodynamic model simulations of aerosol-gas partitioning for sulfate, nitrate, sodium, chloride and water using the ISORROPIA model (Nenes et al., 1998) reveal that observed phase partitioning of the sum of gaseous ammonia and particulate ammonium is reasonably well simulated while phase partitioning of particulate and gaseous nitrate is not. Severe underestimation of particulate nitrate by bulk aerosol models reflects the fact that the $PM_{2.5}$ aerosol is externally mixed, containing acidic submicron sulfate particles and supermicron nitrate particles.

More details of the experimental procedure and its results are provided in an article by Lee et al. (2004).

5.2.2 Short Time Resolution Sulfate Concentrations at Big Bend

As part of the BRAVO Study, continuous high-time-resolution measurements of fine particulate sulfate were made at Big Bend National Park for a 90-day period of August through October. A prototype instrument collected a 10-minute duration humidified sample every 12 minutes by impaction on a nichrome strip. The 2-minute analysis period entails flash heating of the sample to convert the collected particulate sulfate to SO_2, which is subsequently transported to a modified high-sensitivity pulsed UV-fluorescence analyzer for quantification. The nichrome collection substrate was replaced every third day and the system was calibrated using aqueous mixtures of ammonium sulfate and oxalic acid applied directly to the collection substrate and analyzed on a weekly basis. More information about this instrument, its use in the BRAVO Study, and the subsequent data analysis and interpretation by Aerosol Dynamics is provided in the article by Hering et al. (2003).

Comparison of the high-time-resolution sulfate data with collocated integrated, 24-hour filter measurements yielded a linear regression relationship of $y = 0.91x + 0.76$ over the

90-day period, with an $R^2 = 0.78$, where *y* is the 24-hour averaged sulfate concentration from the high-time-resolution analyzer and *x* is the 24-hour duration filter sample sulfate concentration. On a monthly basis, R^2 was 0.88 and 0.90 in August and September, but declined to 0.65 in October. Concurrently, the response to the aqueous standards decreased by 20% by the end of the study, probably due to degradation of the flash system. The reduced response against the aqueous standard was taken into account in the data reduction, but it may have contributed to increased scatter and the poorer correlation. After adjustment, the ratios of mean sulfate concentrations measured by the high time-resolution analyzer to the filter measured concentrations were 1.10, 1.13, and 1.37 for the three months of August through October.

Figure 5-5 is a time plot of hourly particulate sulfate and SO_2 data for the first few days of operation of the high-time-resolution sulfate analyzer. Note the late-night short-term sulfate and SO_2 peaks (August 17 to 21). Other periods had sulfate peaks without corresponding SO_2 peaks (August 22 to 23). Figure 5-6 is a high-time-resolution sulfate time series plot from August 24 through September 5 that shows no consistent diurnal patterns, but does show prominent multi-day incursions of high-sulfate air masses.

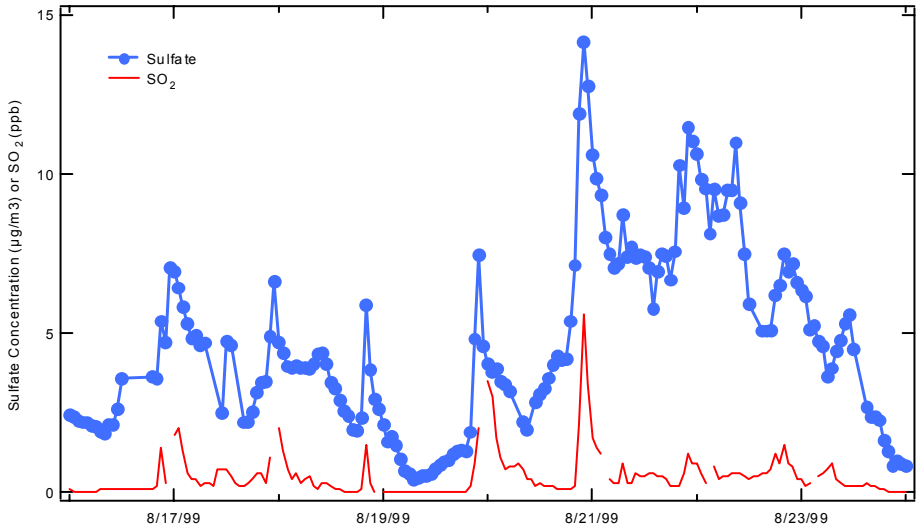

Figure 5-5. *Example of hourly fine sulfate and sulfur dioxide concentration measurements at Big Bend National Park.*

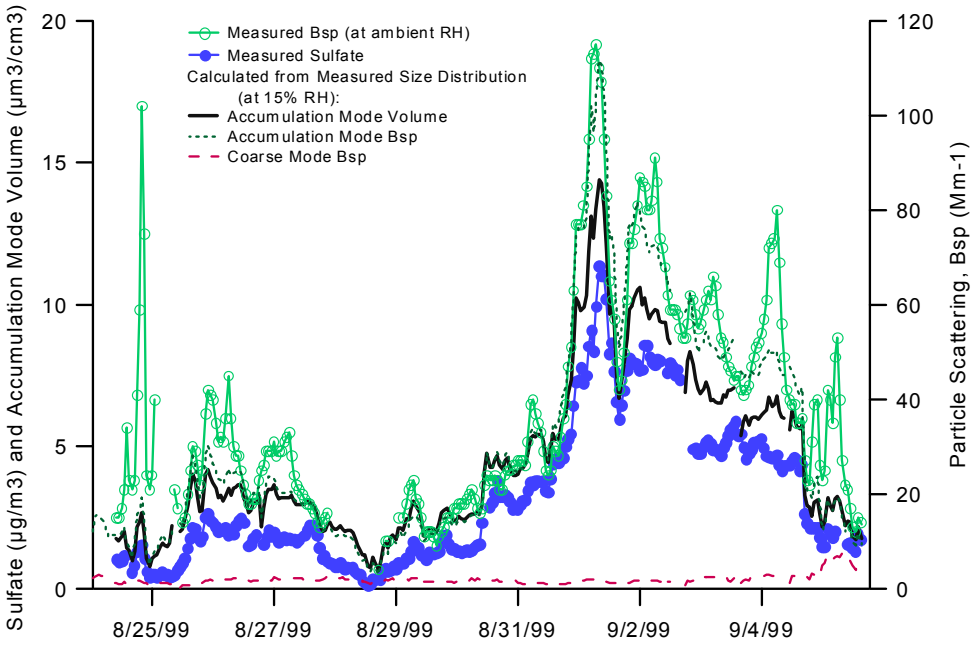

***Figure 5-6**. Example of light scattering coefficient measured at ambient humidity for particles below 2.5 µm, compared with measured hourly-averaged sulfate concentration, accumulation mode volume and light scattering coefficient, and coarse mode particle scattering, all derived from physical size distribution measurements.*

Figure 5-6 also shows good correspondence between the high-time-resolution particulate sulfate concentration and light scattering data as measured by a nephelometer, and even better correlation ($R^2 = 0.96$) to light scattering calculated for the accumulation particle size range from dry particle size distribution data (see Section 5.2.4).[2] The nephelometer-measured light scattering includes the effects of water growth of hygroscopic particulate material such as the sulfate compounds during periods of high relative humidity. Data from the high-time-resolution sulfate analyzer and nephelometer, and accumulation mode particle size distributions information were used in a two-component model to infer the functional dependence of sulfate light scattering on relative humidity. The results are consistent with the water growth curves for ammonium sulfate of Tang and Munkelwitz (1994).

5.2.3 Organic Source Markers in Big Bend Aerosol

$PM_{2.5}$ organic particulate matter samples were collected daily at the K-Bar site in Big Bend National Park. Particulate matter was collected with a modified DRI semi-volatile organic compound sampler on pre-fired quartz fiber filters. The samples were analyzed to identify concentrations of tracers for various types of carbonaceous particulate matter sources.

[2] The physical particle diameter that separates the accumulation and coarse modes averaged 0.77 ± 0.15 µm.

The individual filter samples provided insufficient material for organic speciation, therefore samples were grouped based on their air mass history. Twelve composite samples, each containing 3 to 10 daily samples and labeled as July1, July2, etc., as indicated in Figure 5-7, were analyzed. (See Brown et al. (2002) for the dates included in each composite.) Samples were extracted with dichloromethane and analyzed by gas chromatography coupled to mass spectrometry (GC/MS). The quantification was focused on a series of compounds previously shown to serve as particle phase tracers for various carbonaceous aerosol sources. Approximately one hundred organic compounds comprising n-alkanes, n-alkanoic acids, polyaromatic hydrocarbons as well as specific source marker compounds including methoxyphenols and sugar anhydrides (related to wood smoke), hopanes and steranes (vehicle emissions) and cholesterol (meat cooking) were routinely determined. These targeted compounds together accounted for 1 to 6% of the total fine particulate organic matter.

The n-alkane carbon preference index (CPI), which is defined as the sum of the concentrations of odd-carbon-number alkanes divided by the sum of the concentrations of the even-numbered alkanes, is commonly used to assess the importance of biogenic vs. fossil fuel contributions to emissions of n-alkanes. This indicator suggested low contributions of primary biogenic material during the first three months of the study, while in October air masses advecting from north and south were more strongly influenced by biogenic sources. Values of the CPI were closest to 1.0, the value expected for combustion emissions of n-alkanes, during periods when the K-Bar OC concentrations were highest (see Figure 5-7). This result indicated the importance of anthropogenic emissions during periods of high local organic aerosol concentrations.

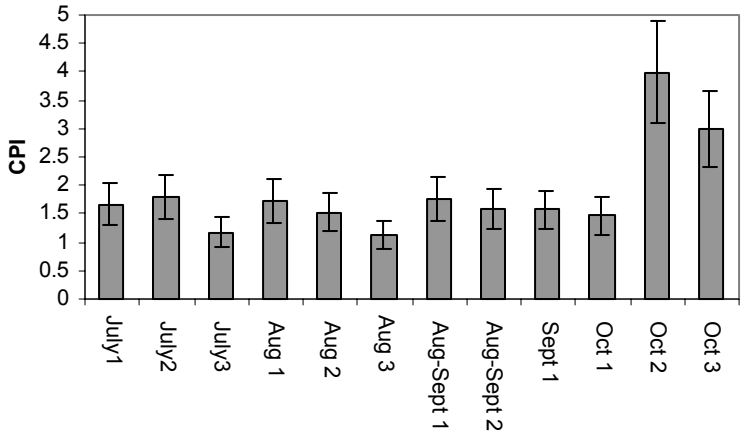

Figure 5-7. *The n-alkane carbon preference index (CPI) for the BRAVO organic aerosol sample composites. The lowest CPI values are seen for the composites labeled July3 and August3, which also had the highest OC concentrations.*

Molecular source marker concentrations were generally below or close to their detection limits, suggesting very low contributions of the corresponding primary sources to the ambient carbonaceous aerosol in Big Bend National Park. Upper bounds to source contributions were estimated assuming a maximum tracer concentration equal to the detection limit of the species. The upper limit for vehicular exhaust, using hopane as a tracer, varied from 1 to 4% with a median value of 1.5%.

Wood smoke was not identified by these methods as a significant contributor to the carbonaceous aerosol during the BRAVO Study period. Using levoglucosan concentrations, typical estimated wood smoke contributions were lower than 1%. Detection of other wood smoke marker compounds, however, questions the validity of the use of levoglucosan as a conservative tracer. Source apportionment using vanillin as a tracer indicated up to approximately 6% of the particulate organic matter being derived from wood smoke. The difference in wood smoke contribution estimates may reflect degradation of levoglucosan during transport in the presence of acidic aerosols and/or secondary production of other markers like vanillin.

A number of indicators, including low source contributions of primary compounds and absence of marker compounds, suggest that a large portion of the organic aerosol present during BRAVO was secondary. Comparisons of observed OC/EC ratios with wintertime OC/EC ratios in the park (see Brown et al. (2002) for details) suggest that frequently more than half of the OC observed during BRAVO was secondary in origin.

Findings from this investigation reveal the limitations to performing quantitative source apportionment of carbonaceous aerosols in remote locations, where concentrations are low and significant conversion to secondary organics has taken place. To refine the method, future work is needed to evaluate the stability of common organic source markers during long-range transport and the production of secondary organic carbon. More details on the experiment and the data analyses described above are provided in an article by Brown et al. (2002).

5.2.4 Particle Size Distribution

Dry particle size distributions were measured with 15 min resolution over the size range of $0.05 < Dp < 20$ μm from July to October 1999 at the K-Bar site in Big Bend National Park. Three instruments were used to cover this size range: a differential mobility analyzer (0.05–0.87 μm), an optical particle counter (0.1–1.0 μm), and an aerodynamic particle sizer (0.5–20 μm). A new method was developed to align the individual instrument size distributions in overlap regions, thereby producing a single, merged size distribution from the data (Hand and Kreidenweis, 2002). As part of this alignment method, estimates of dry aerosol refractive index (study average, 1.566 for the fine mode) and effective dry particle density (study average, 1.56 g cm^{-3}) were retrieved. The retrieved estimates agreed well with properties computed from 24-hour particulate chemical composition measurements.

Statistics for the particle size distributions were computed for accumulation, coarse, and occasionally giant, modes, where the modes were distinguished by minima in the observed distributions. As shown in Figure 5-8, coarse mode particulate matter volume concentrations contributed significantly to total particulate matter volume concentrations during July and August, when episodic North African dust outbreaks were detected. During the first half of the study, the geometric mean volume diameter for the coarse mode was smaller than during the second half, reflecting the non-local sources of the dust. The study-average particulate matter volume concentrations were 3 ± 2 and 4 ± 4 $\mu m^3/cm^3$ for the accumulation and coarse modes, respectively, with peak values of accumulation mode

volume concentrations occurring from mid-August through mid-October. Geometric volume mean diameters for the accumulation and coarse particle modes were 0.26 ± 0.04 and 3.4 ± 0.8 µm, respectively.

Further details about the size distribution measurements are contained in the article by Hand et al. (2002**).**

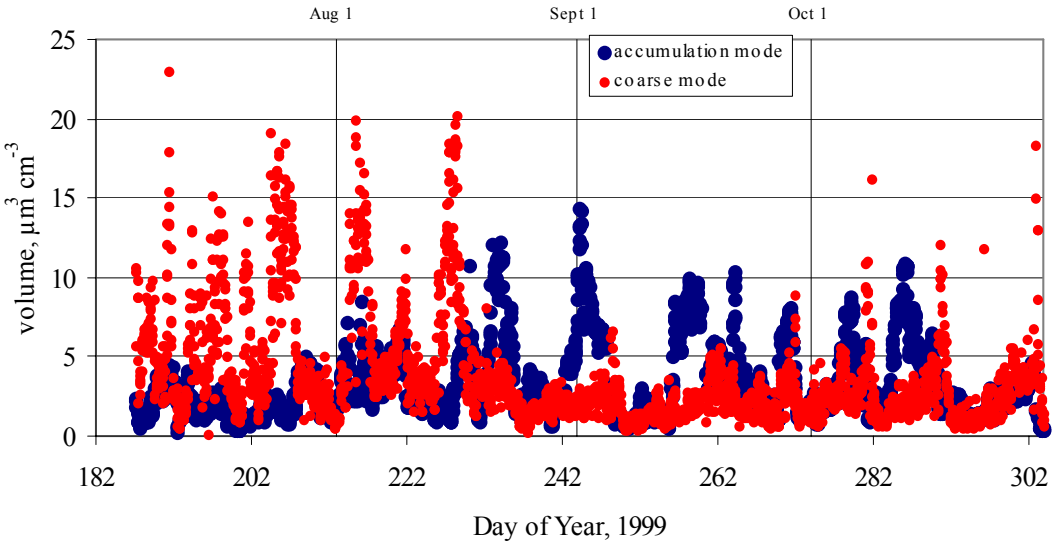

Figure 5-8. *Timelines of dry particulate matter volume concentrations (in µm³/cm³) at Big Bend National Park for the accumulation and coarse modes, as computed from measured size distributions. Day 182 is July 1, and day 304 is October 31.*

5.2.5 Very Fine PM as a Source Tracer

Primary particles from high temperature sources tend to form very fine and ultra-fine particles that reflect the source materials. Normally, very fine (D_p <0.26 µm) and ultra-fine (D_p < 0.1 µm) particles have a short lifetime due to high diffusion rates, but in some cases, such as rapid dilution into the clean, dry conditions seen in the southwest U.S., they can persist and become an important component of the ambient aerosol (Cahill et al., 1993). Near Big Bend NP there are many such potential sources, including coal-fired power plants and industrial sources, in both the U.S. and Mexico. Such large point sources, however, often produce relatively narrow plumes of particles that may affect a receptor site for a limited duration, requiring highly time resolved as well as size resolved data. In order to establish transport patterns into Big Bend NP during BRAVO, a study was carried out to collect and analyze very fine particles by size, time, and composition.

Particles were collected in an 8-stage rotating drum impactor (Raabe et al., 1988) modified to a slotted configuration and with cut points of 12 to 5, 2.5, 1.15, 0.75, 0.56, 0.34, 0.26, and 0.09 µm aerodynamic diameter. The flow was held at 10 l/min by the final slot,

which was a critical orifice. The rotation rate was 6 mm/day, which over four weeks produced eight Apiezon-greased Mylar strips each 168 mm long. The strips, representing the finest particles, $0.26 > D_p > 0.09$ µm, were analyzed on the University of California at Davis DELTA Group synchrotron x-ray fluorescence (S-XRF) microprobe (Bench et al., 2002). The extremely high x-ray flux and 100% polarization allowed highly sensitive measurements of all elements sodium and heavier, to a few pg/m^3, although elements heavier than molybdenum and lighter than gold are often interfered with by more abundant light elements. The seven larger-particle DRUM strips were archived and have not been analyzed.

The results for two of the most abundant very fine elements, silicon and sulfur, are shown in Figure 5-9 for August 1999. Generally, the average concentrations of these particles are very low, (Si = 0.14 ng/m^3, S = 1.88 ng/m^3) with the very fine sulfur (presumably sulfate) a small fraction of $PM_{2.5}$ sulfate. However, on occasion, sharp increases in both very fine Si and S occur, always in correlation ($r^2 = 0.95$ for August, for example). Comparison with high resolution $PM_{2.5}$ sulfate data show that on one occasion, August 18, there were three hours in which almost all of the $PM_{2.5}$ sulfate was in the very fine size range. The silicon is not accompanied by other crustal elements (enrichment factor vs. aluminum is ~20) but is probably derived from the same processes as the "large glassy plerospheres" long associated with coal-fired power plants. (The postulated formation mechanism is $SiO_2 \rightarrow SiO$ in the reducing fuel rich region of combustion, then oxidation to SiO_2 in the flame, followed by rapid condensation to very fine glassy mist that can form very fine particles, some of which agglomerate into the large plerospheres.) The sulfur in the largest peaks is probably H_2SO_4, based on hydrated droplets seen even after vacuum, which argues against long-range transport.

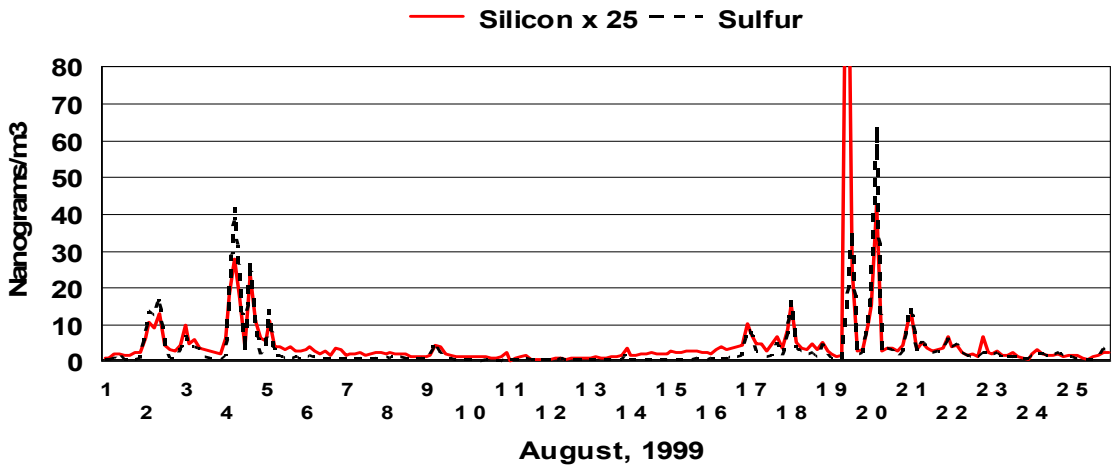

Figure 5-9. *Timeline of very fine (0.26 µm > D_p > 0.09 µm) silicon (x 25) and sulfur concentrations at Big Bend National Park during August 1999.*

HYSPLIT4 isentropic backward trajectory analyses at 500, 1,000, and 2,000 m AGL for these events show that the largest of these events in early and late August occurred with

slow southeast winds up the Rio Grande Valley, in many cases passing within a few kilometers of the *Carbón* power plants in Mexico.

HYSPLIT analysis was also used to study the vertical stability of the atmosphere and to examine the conditions under which the elevated plume could ventilate down to ground level. It is unlikely that these very fine particles could long survive in high humidity conditions such as over the Gulf of Mexico or the eastern US. On one occasion, and only for one hour, (August 4, 11 AM) a plume was observed that contained a complex mixture of very fine elements Si, S, Ca, Fe, As, K, Cu, Zn, and Se, the latter 7 of which are absent from typical pure Si/S plumes. We interpret this as indicating an additional high temperature source or sources that, from trajectory analysis, could be the city of Monterrey, Mexico.

The high $PM_{2.5}$ sulfate episodes of September and October did not have strong very fine Si and S signatures. Thus, if they were from coal-fired power plants, they were much farther away than *Carbón,* or the meteorology had changed and resulted in destruction of the very fine plume, perhaps by particle growth in high humidity. The latter explanation is less plausible than the former since the silicon, almost certainly in non-hydrophilic glassy particles, was also missing from the aerosol.

In summary, whenever very fine and highly correlated Si and S are present, without other trace elements, this investigation suggests influence from coal-fired power plant emissions. However, the absence of such particles does not necessarily imply that there is no influence from coal-fired power plants, as these very fine particles would not survive long-range transport in humid conditions.

Further information concerning this work can be found in a report by Cahill et al. (2003), which is contained in the Appendix

5.3 Characterization of Optical Conditions at Big Bend National Park

Direct measurements of total light extinction, light scattering by particles (both at ambient conditions and dried) and of particle absorption of light were made at the K-Bar site at Big Bend National Park. In addition, the light extinction due to the components of the aerosol was estimated. The key findings of these measurements and analyses of optical conditions are presented here.

The discussion below summarizes the following two topics, both at Big Bend National Park:

- Comparison of light absorption measurements by three methods
- Measurements of optical properties of the atmosphere

5.3.1 Light Absorption Measurements

Particulate matter light absorption at Big Bend was measured by both a photoacoustic instrument and an aethalometer (an automatic filter-based absorption measurement method). Both instruments operated simultaneously for one month (mid-September to mid-October),

enabling comparison of their measurements. Concurrently, the routine BRAVO sampling included analysis of 24-hr filter samples for light-absorbing carbon.

The basic design of the photoacoustic instrument operated by DRI was an update of the instrument described by Arnott et al. (1999). The sample inlet included a 2.5 μm cut point cyclone (URG) and an annular denuder (URG model 962) coated with MnO_2 to take out NO_2 that might otherwise produce a photoacoustic signal from light absorption in the green wavelength region. The minimum detection limit (MDL) of the instrument used in the BRAVO Study was 0.5 Mm^{-1} for an integration time of 8 minutes.

A Magee Scientific aethalometer (Model AE-16) was operated by CSU continuously during the study. The aethalometer measures the concentration of absorbing aerosol by measuring the optical attenuation of light caused by a particulate matter sample deposited continuously on quartz fiber filter tape. It is assumed that aerosol absorption is due mainly to carbonaceous particles (referred to here as black carbon, BC). A beam of light is directed at the aerosol deposit spot on the tape and the attenuation of light due to aerosol absorption is measured by detection of transmitted light through the sample on the filter.

After the BRAVO field study, the minimum detection limit of the aethalometer was determined at the Atmospheric Simulation Laboratory at Colorado State University. Particle-free air was delivered to the instrument and from these measurements the MDL was determined to be 71 ng/m^3 for an hourly average**.**

Figure 5-10 compares time series of photoacoustic measurements, as 12-hour averages, with aethalometer BC measurements (top) and IMPROVE elemental carbon measurements. (The relative scaling of photoacoustic absorption and aethalometer BC concentration axes in the top plot was based on the linear regression described below. The same scaling was used in the lower plot.)

The top panel of Figure 5-10 shows that the maximum light absorption was 2.1 Mm^{-1}, and the maximum black carbon concentration was 0.2 $\mu g/m^3$, consistent with other measurements in the arid southwest U.S. (Pinnick et al., 1993). Between September 20-23, the temporal variations of the measurements are very similar. Around September 25 and October 2, both measurements indicate low values, and the aethalometer measurements are smoother than the photoacoustic measurements. During October 8-16, the photoacoustic measure of light absorption is proportionally lower than the aethalometer measure of black carbon. In summary, there are periods of agreement and disagreement in the relative trends of black carbon measurements by the two methods, perhaps due to compositional changes and to the difference in the detection limits of the methods.

The lower panel of Figure 5-10 compares photoacoustic aerosol light absorption measurements with IMPROVE elemental carbon (light absorbing carbon) concentration measurements. Note that the EC signal is noisier than the BC signal. Also note that relatively good agreement in this panel is found around October 8, though relatively poor agreement is found near October 17. Owing to the relatively low signal levels at this site, firm statistically sound conclusions cannot be drawn from this data set. However, one could state that use of the conventional light absorption efficiency factor of 10 m^2/g for the IMPROVE EC measurements places IMPROVE absorption values into the same ballpark as the photoacoustic measurements of aerosol light absorption.

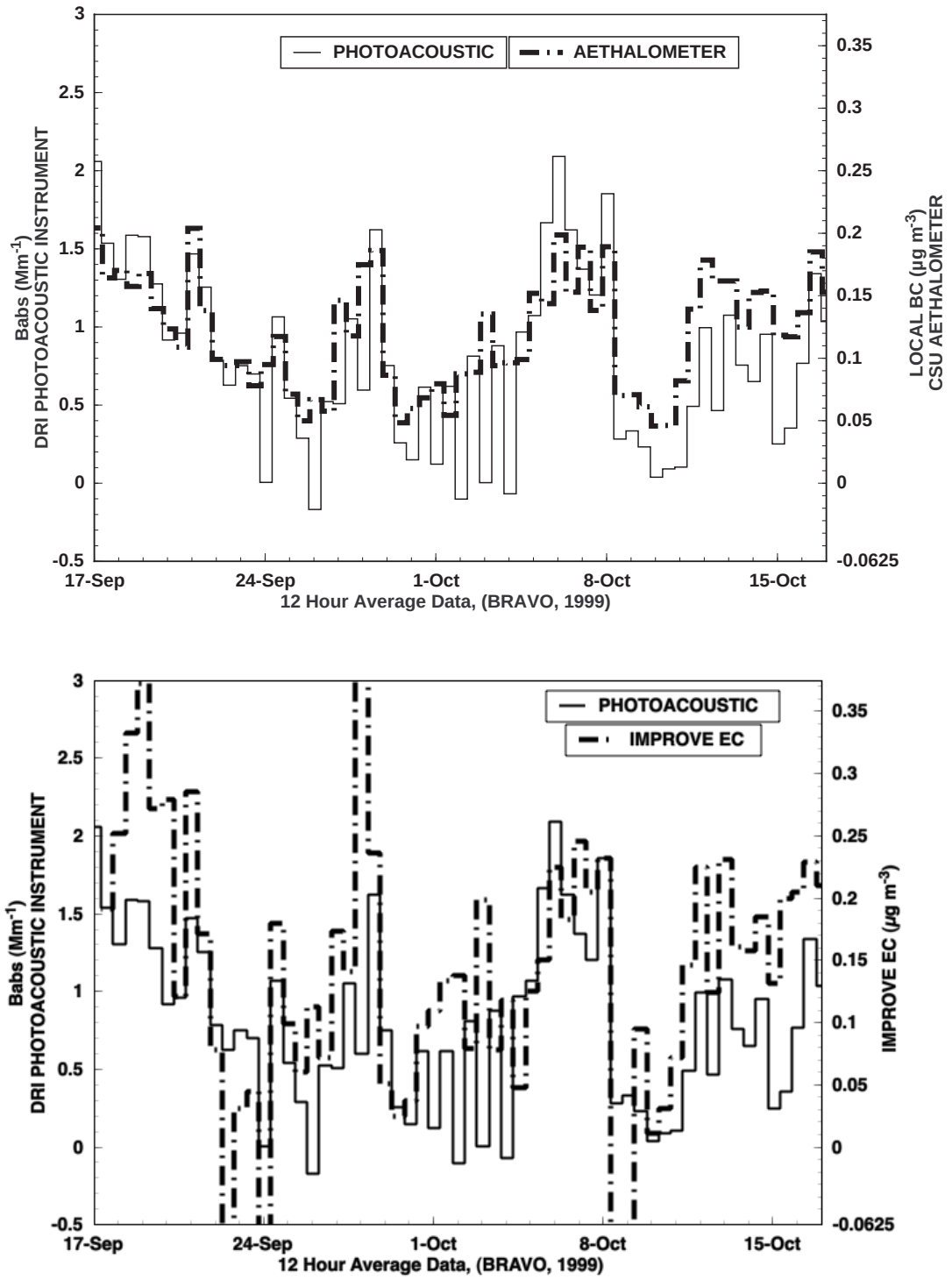

Figure 5-10. *Comparisons of 12-hour averages of the photoacoustic light absorption measurements and the aethalometer black carbon measurements (top) and IMPROVE EC measurements (bottom) during the BRAVO Study. The black carbon and EC concentrations were scaled to the pressure and temperature of the site for direct comparison with photoacoustic data.*

Photoacoustic light absorption measurements are plotted against aethalometer black carbon measurements in the scatter diagram in Figure 5-11. The slopes of the linear models are 8.4 m^2/g and 9.9 m^2/g, depending on whether the entire data set is considered (solid line), or just the data corresponding to BC > 0.15 $\mu g/m^3$ are used. (The corresponding R^2 values are 0.45 and 0.21, respectively.) The first slope represents the value that can occur when measurements are near the noise floors of the instruments. A prior study comparing versions of these two instruments at a mostly urban-aerosol-dominated site in Brighton, CO (Moosmüller et al., 1998) indicated an efficiency factor of 10.0 m^2/g, which agrees with the value obtained at Big Bend when the black carbon concentration was greater than 0.15 $\mu g/m^3$. It also agrees with the conventional value that is used, for example, in the IMPROVE formula for estimating extinction from particulate matter component concentrations.

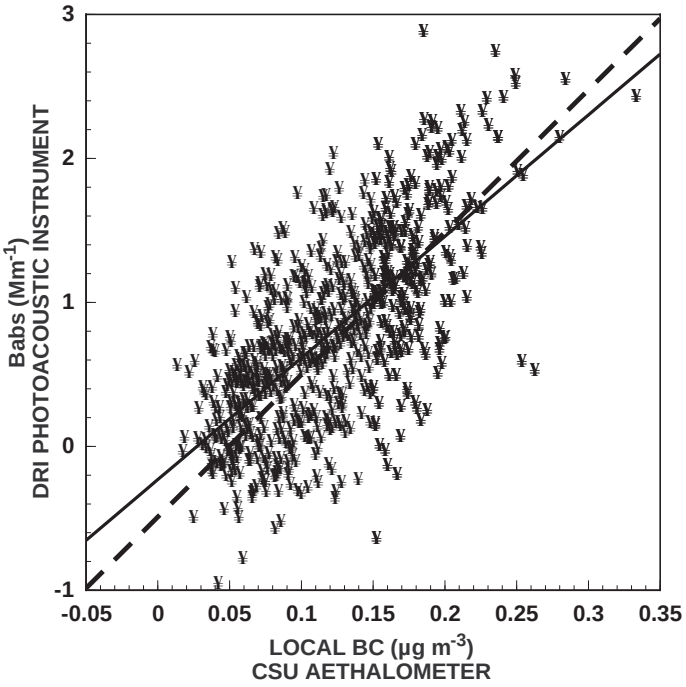

Figure 5-11. *Comparison of hourly averaged black carbon and light absorption measurements during the BRAVO study time period of Figure 5-10. Linear regression lines are for the entire data set (solid) and just the data where BC > 0.15 µg/m³ (dashed).*

One can interpret these slopes as absorption efficiency factors to use for estimating light absorption from aethalometer measurements of black carbon. (Note that aethalometer black carbon concentrations are themselves derived from apparent filter absorption by using an empirical efficiency factor of 19 m^2/g, as discussed by Bodhaine (1995). The multiple-scattering filter substrate tends to amplify light absorption beyond the in-situ value, which is a well-known characteristic of the aethalometer.)

The coefficient of determination (R^2) of the data in Figure 5-11 is relatively small (0.45), which appears to be a consequence of the low concentrations of light absorbing species at Big Bend. The aethalometer BC values never go to zero because values below the minimum detection limit of the instrument were not included in the analysis.

This experiment showed that fast time-response light absorption measurements were feasible and that there was reasonable consistency between absorption determined from IMPROVE elemental carbon (or LAC) measurements on filters using the conventional efficiency of 10 m^2/g, absorption derived from aethalometer measurements, and the photoacoustic measurements. (Comparison with the integrating sphere absorption measurements made by IMPROVE for many years was not addressed.)

5.3.2 Optical Measurements of the Big Bend Atmosphere

The optical properties of the atmosphere at Big Bend National Park during the full period of the BRAVO Study were measured routinely in multiple ways. Light extinction was measured by transmissometers. Open-air nephelometry was used to measure ambient light scattering. (The difference between extinction and scattering is one measure of light absorption.) In addition, light scattering by particles smaller than 2.5 μm was measured, both under ambient relative humidity and for a dried aerosol. Fine and coarse particle absorption were estimated from light-absorbing carbon (LAC) measurements on $PM_{2.5}$ and PM_{10} filter samples; absorption was also measured with an aethalometer.

Optec LPV-2 transmissometers were used to determine ambient light extinction. Their use in remote locations such as national parks is discussed by Molenar et al. (1989), while Dietrich et al. (1989) presents their use in urban settings. Careful operation of the transmissometer (daily cleaning of optics and pre- and post-calibrations) should result in extinction measurements with an accuracy of about 10% (Molenar et al., 1989).

Five Optec NGN-2 integrating nephelometers, in various configurations, were operated at Big Bend during the study. Details of ambient nephelometer measurements were covered in Malm et al. (1994) and Day et al. (1997). Two nephelometers utilized the open-air configuration and were operated using IMPROVE protocols (Air Resource Specialists, 1995). The remaining instruments were modified for specialized measurements. One nephelometer was fitted with an Anderson PM_{10} inlet and the other two operated at reduced flow rate (113 l/min) and each was fitted with a Bendix-240 cyclone with a 2.5 μm cutpoint.

In addition to the Optec instruments, a Radiance Research M903 integrating nephelometer was configured to measure scattering by dried $PM_{2.5}$. Sample air was drawn through a temperature controlled humidity conditioner and passed into the nephelometer. The humidity conditioner consisted of Permapure Nafion dryers; placing the dryers in a constant temperature water bath controlled their temperature.

Three Rotronics mp 100f combination relative humidity and temperature sensors were housed in PVC holders and aspirated by a fan. The manufacturer reports the accuracy of the relative humidity sensor to be ±2%.

The results of these measurements are presented in detail in the CIRA/NPS report (Schichtel et al., 2004), which is included in the Appendix. The discussion below summarizes the key findings.

Table 5-3 summarizes the optical measurements. The extinction measurements, b_{ext}, were made with a transmissometer. The b_{ext} values given in Table 5-3 represent the portion due to particles alone, i.e., Rayleigh scattering by air molecules has been subtracted. The measurements of the scattering coefficients $b_{sp,open}$, $b_{sp,10\mu m}$ $b_{sp,2.5\mu m}$, and $b_{sp,dry}$ were made, respectively, with an open air nephelometer, the nephelometer fitted with a PM_{10} inlet, a nephelometer fitted with a 2.5 µm inlet, and the nephelometer that had a 2.5 µm inlet that dried the aerosol. The absorption measurements referred to in this table were estimated from light absorbing carbon measurements in the fine and coarse (PM_{10}-$PM_{2.5}$) modes.

Table 5-3. Summary of measurements of particle absorption and scattering (in Mm^{-1}) at Big Bend National Park.

Variable	Mean	Standard Deviation	Minimum	Maximum
b_{ext}	29.25	19.66	3.58	71.96
$b_{abs,2.5\mu m}$	1.32	0.62	0.36	2.51
$b_{abs,coarse}$	0.87	1.05	-1.26	3.05
$b_{sp,open}$	24.16	16.20	6.66	63.54
$b_{sp,pm10}$	25.11	17.25	6.12	65.71
$b_{sp,2.5}$	21.88	15.91	4.49	61.87
$b_{sp,2.5,dry}$	17.74	13.47	2.91	53.76
b_{ext} - $b_{sp,open}$	5.09	5.09	-3.94	16.16
$b_{sp,open}$ - $b_{sp,2.5}$	2.29	1.22	0.65	8.07
$b_{sp,2.5}$ - $b_{sp,2.5,dry}$	4.14	3.46	0.58	17.87

Table 5-3 shows that the average b_{ext} was 29.25 Mm^{-1}, which corresponds to a standard visual range of 100 km and a haze index of about 14 deciviews. The average b_{ext} exceeds $b_{sp,open}$ by about 5.1 Mm^{-1} and exceeds $b_{sp,2.5\mu m}$ by about 7.4 Mm^{-1}. These values are 17% and 25% of particulate extinction, respectively, indicating that scattering by all particles accounts for about 83% of the particle extinction and that by fine particles alone accounts for about 75% of the light extinction, on average. All of these scattering figures include the contribution of water contained in the particles. Scattering by dry particles accounts for 61% of the light extinction. Absorption, fine plus coarse, makes up another 8%.

However, summing average $b_{sp,2.5\mu m}$, $b_{sp,coarse}$, and coarse and fine absorption yields 26.38 Mm^{-1}, which is 2.87 Mm^{-1} or 10% short of measured extinction. Coarse particle scattering ($b_{sp,open}$ - $b_{sp,2.5\mu m}$) is estimated to be 2.29 Mm^{-1}. Coarse particle scattering is known to be underestimated by about a factor of one third to a half by integrating nephelometers because of forward angle truncation errors (Molenar, 1997); doubling coarse particle scattering would approximately make up for the underestimated or missing extinction. Such doubling has not been applied here.

Finally, the increase in fine particle scattering due to water associated with hygroscopic particles is 4.14 Mm^{-1}, or about 14% of total extinction.

Based on Table 5-3 and the discussion above, Figure 5-12 illustrates the fraction each measured component contributed to the average transmissometer-measured total extinction at Big Bend during the BRAVO Study.

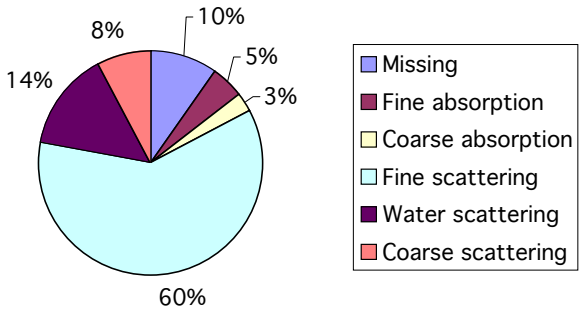

Figure 5-12. *Average distribution of the measured components of extinction at Big Bend during the BRAVO Study period*
.

5.4 Meteorology During the BRAVO Study

In this section the meteorological conditions during the BRAVO Study are briefly described. Emphasis is placed upon wind patterns and transport pathways.

A summary of July to October 1999 wind direction frequency from the BRAVO radar wind profilers (RWPs) is shown in Figure 5-13. At all locations, wind directions are more variable at the higher levels (>1500 m). Big Bend has mainly southerly winds at the 0-500 m level, the frequency enhanced by channeling due to local terrain. Eagle Pass and Brownsville show a high frequency of southeasterly winds, especially below 1500 m. At Llano winds below 1500 m are predominantly from the south, with more northerly winds above 1500 m. The Llano winds reflect the northward transport on the west side of the "Bermuda High" high pressure region, which is illustrated in Figure 5-14.

Back trajectory analysis showed persistent transport from the southeast during July. Such flow was typically relatively rapid and was in response to clockwise rotation around the Bermuda/Azores High pressure systems (Figure 5-14). This pattern explains why July is the peak month for fine soil at Big Bend due to transport of Saharan dust.

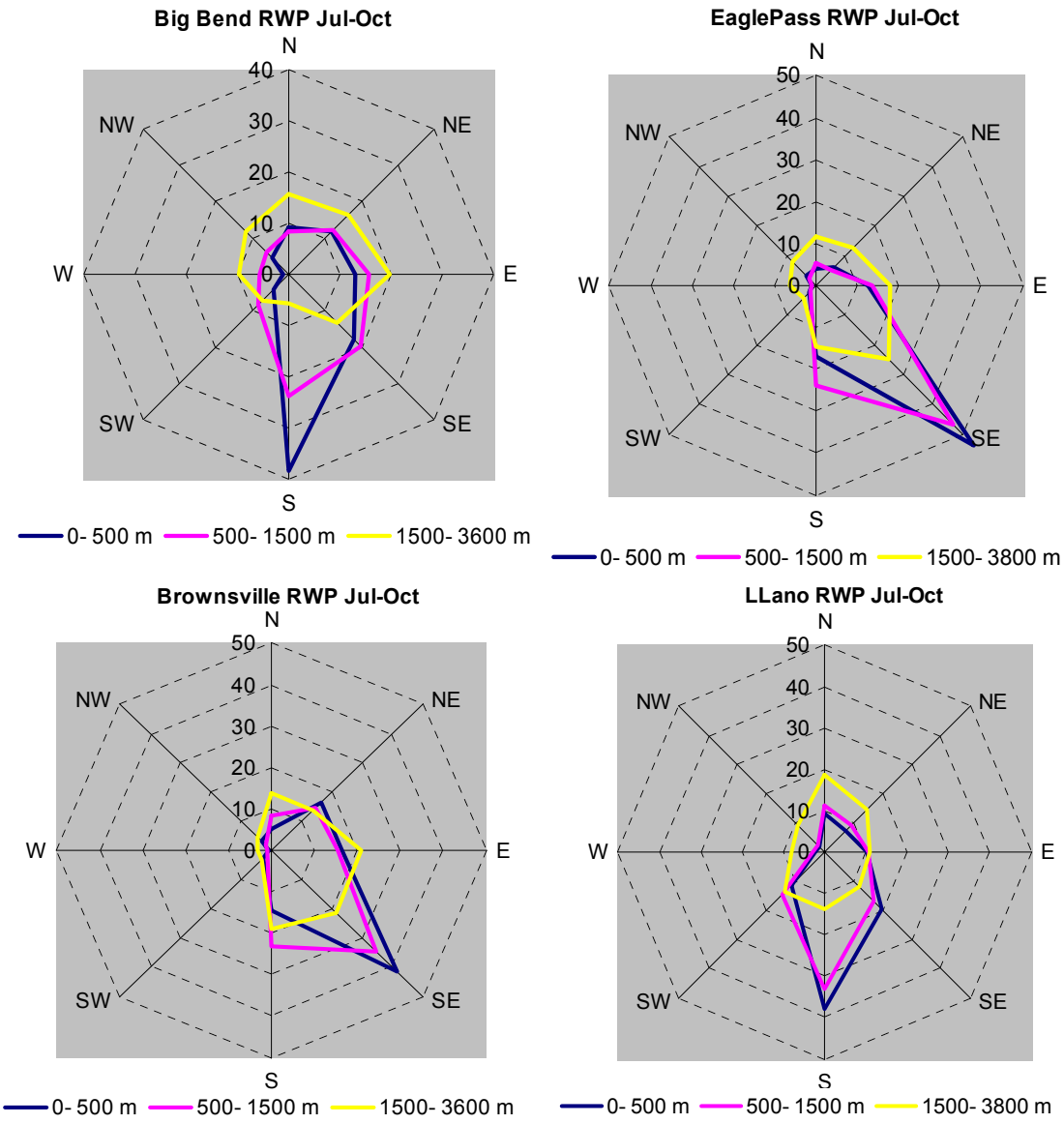

Figure 5-13. *Frequencies of wind directions at three height ranges during July-October 1999, as measured by the BRAVO radar wind profilers.*

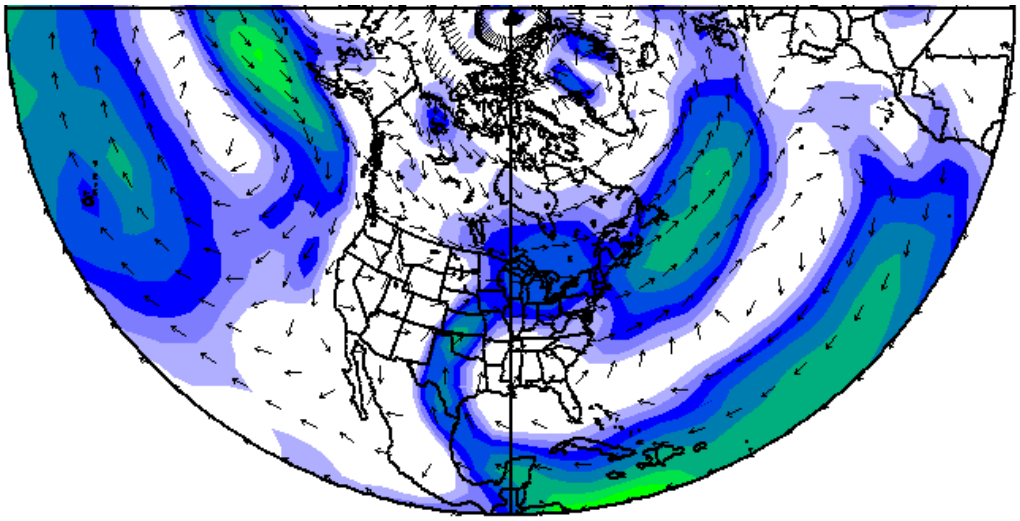

Figure 5-14. *July 1999 monthly resultant winds at 850 mb (approximately1500 m MSL), showing flow from the south in the Big Bend area. Source: NOAA Climate Diagnostics Center.*

During August the transport speeds weakened and some transport from the northeast was noted. This was evident in the August 20-22 episode of high particulate sulfur at Big Bend, when a high-pressure system over the northern Great Lakes drifted to the southeast. A weak cold front stretched from the North Carolina Coast to South-Central Texas on August 20-21, with light northeasterly flow north of the front, as shown in the weather map in Figure 5-15. On August 22, Category 4 Hurricane Bret made landfall on the south Texas coast. The storm moved northwest toward Big Bend over the next two days causing heavy rains.

The period of August 31- September 3 also had poor visibility. In the period around August 27, stagnant conditions and widespread haze occurred in the Ohio River Valley. A high pressure center over Manitoba, Canada on August 26 moved southeast to northern New York State on August 31. Circulation around the high caused flow from the northeast north of the front and from the east south of the front. By the morning of August 29 many National Weather Service stations in the southeastern US (south of the cold front) were reporting haze, as indicated in Figure 5-16 (haze is denoted by the infinity symbol). Wind conditions were such that the haze was being transported toward Big Bend National Park, with the hazy air mass arriving on August 31.

National Weather Service data indicated widespread haze, especially on the morning of September 1 with visibilities as low as:

- San Antonio 5 miles at 8 am
- Harlingen 3 miles at 7 am
- Laredo 6 miles at 7 am

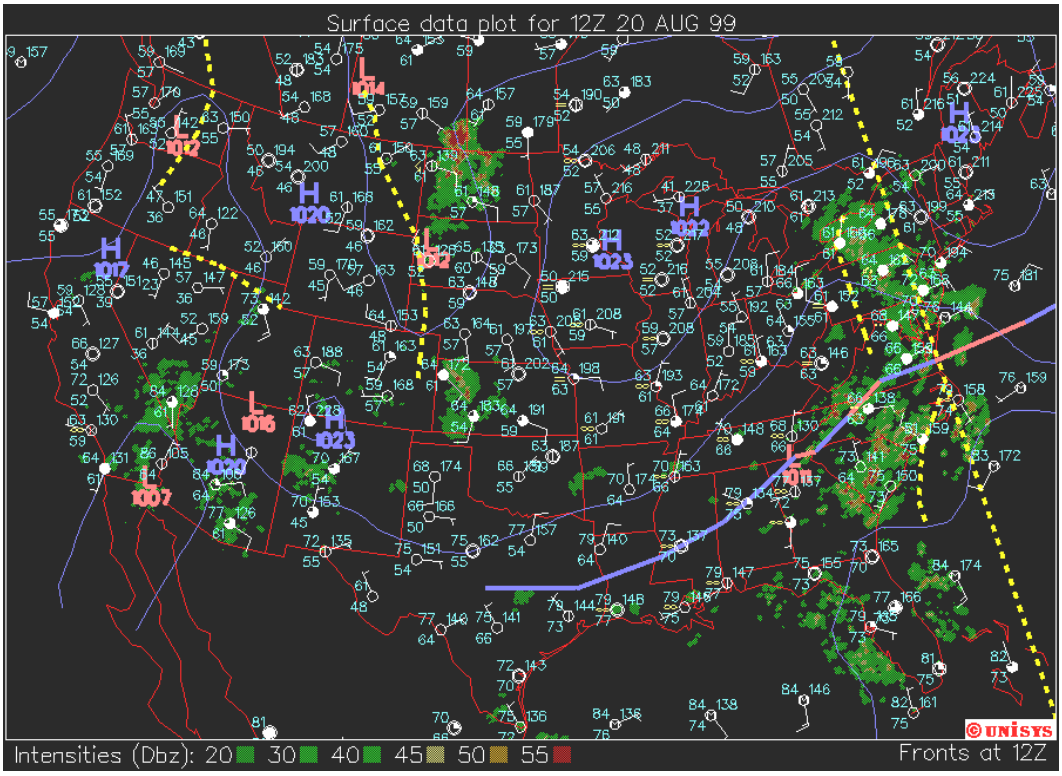

Figure 5-15. *Surface weather map for 6 am CST on August 20, 1999.*

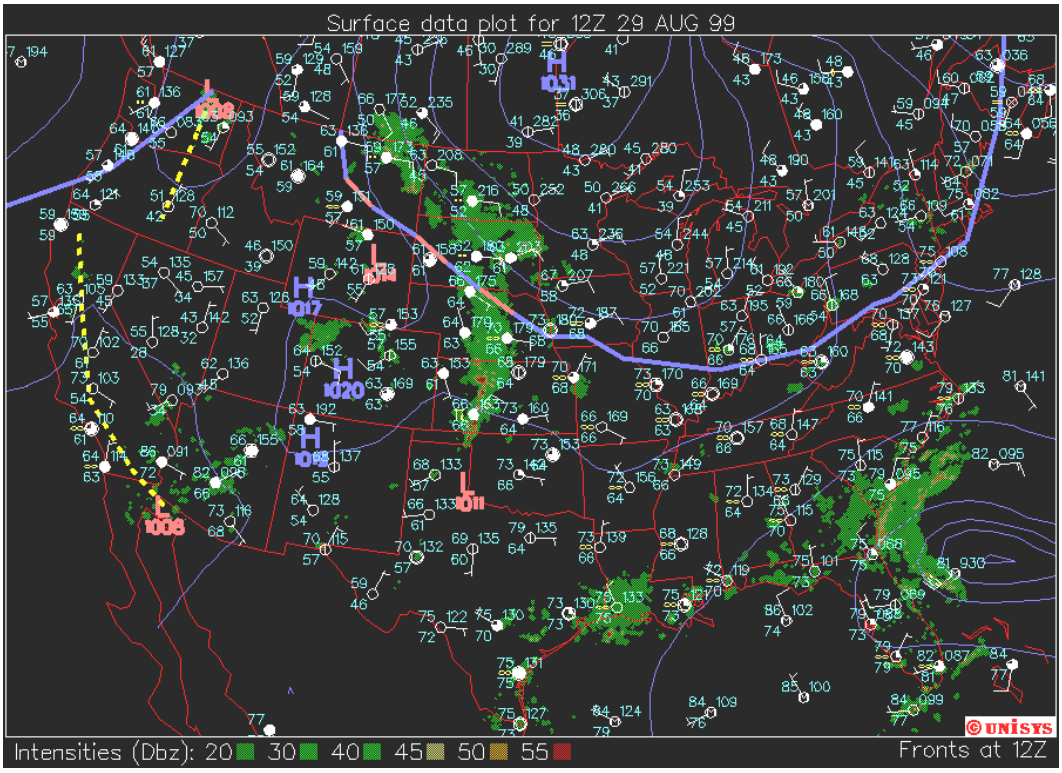

Figure 5-16. *Surface weather map for 6 am CST on August 29, 1999.*

- Del Rio 4 miles at 7 am
- Corpus Christi 3 miles at 7 am (versus 1/4 mile and fog on 8/31).

Conditions were humid with dew point depressions of 0-3 degrees centigrade at these locations. However, relative humidity (RH) at Big Bend was not high during the episode, with RH ranging from about 20% in the afternoons to about 60% in the mornings.

During September and October an increasing number of fronts affected the study area. This resulted in increased occurrence of flows with a component from the north (west-northwest clockwise through east-northeast).

A period of poor visibility and high particulate sulfur occurred from September 13-15. On the afternoon of September 11, wind directions in Texas were generally from the southeast (Figure 5-17), transporting east Texas emissions toward central Texas. By the afternoon of September 13, a weak cold front passed through, bringing east to northeasterly winds over most of Texas as shown in Figure 5-18, transporting haze into the Big Bend area. This period also had high relative humidity at Big Bend, with morning RH from 80-90% and afternoon minimum RH about 40%.

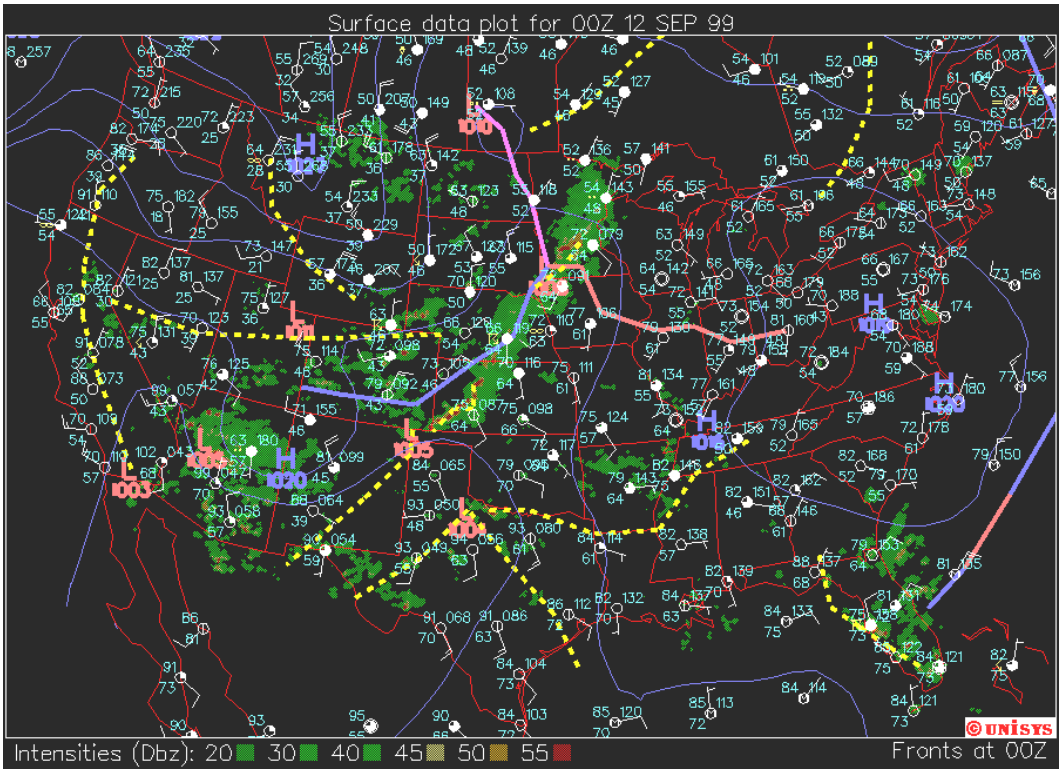

Figure 5-17. *Surface weather map for 6 pm CST on September 11, 1999.*

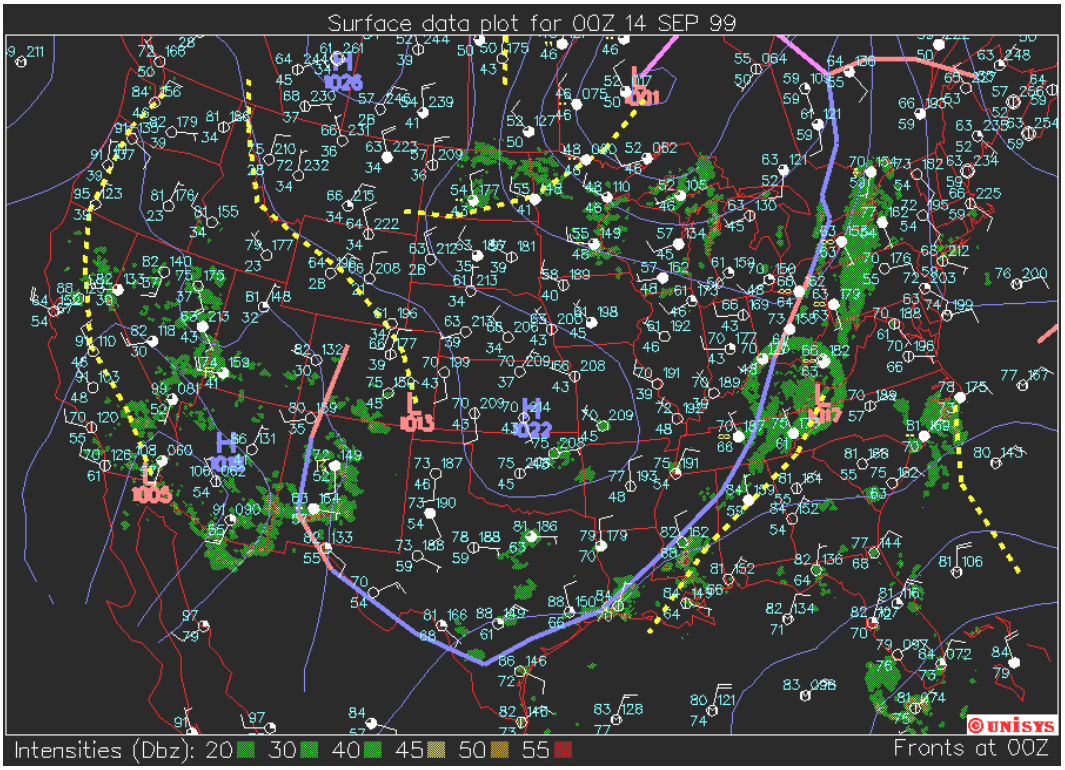

Figure 5-18. *Surface weather map for 6 pm CST on September 13, 1999.*

5.5 Perfluorocarbon Tracer Experiment Findings

Four different perfluorocarbon tracers were released at various locations in the study area throughout the 4-month study period and their ambient concentrations were measured at multiple locations, as described in Section 3.2 and Figure 3-2 in Section 3.3. Here we describe the results of the tracer study, first for the continuously-released tracers and then for the timing tracers. The use of the tracer data for model evaluation is discussed later in this report, in Chapter 9.

5.5.1 Continuous Tracer Results

Table 5-4 provides a summary of the performance of the measurements of the continuously released tracers at the 6-hour sites. In that table, influence functions (IF) were calculated by dividing the tracer concentration by the release rate (i.e., in modeler's notation, IF = χ/Q, where χ is the concentration and Q is the release rate).

Table 5-4. Summary of tracer data at the 6-hour sampling sites. Shown are the percentage of observations with concentrations greater than 2 times analytical uncertainty, the 90th percentile influence function (χ/Q) in 10^{-11} s/m^3, and the distance of the monitoring site from the tracer release location. Sites are listed in order from north to south.

Receptor Site	Tracer release location											
	Eagle Pass			NE Texas			San Antonio			Houston		
	>2σ	90% IF	Dist. (km)	>2σ	90% IF	Dist. (km)	>2σ	90% IF	Dist. (km)	>2σ	90% IF	Dist. (km)
MONA	59%	110	364	9.9	8.2	640	28%	13	469	11%	7.9	731
FTST	50%	97	323	7.5	5.8	658	28%	8.8	453	12%	12	729
MARA	48%	110	302	4.8	3.4	708	34%	11	464	12%	11	755
PRSG	37%	94	274	9.5	4.9	723	20%	9.2	454	10%	9.6	750
BIBE	22%	31	264	0.9	1.9	738	30%	12	455	10%	7.8	754
SNVI	16%	15	247	2.7	1.9	734	15%	5.0	442	1.0%	5.3	742

As indicated in Table 5-4, the Eagle Pass tracer (ocPDCH) was detected above background the most frequently; and sites to the north had greater frequency of elevated concentrations than sites further south, such as Big Bend. This indicates the predominant flow direction was from the southeast. Although the sites to the south (Big Bend area sites) were closer to Eagle Pass than the northerly sites, the northerly sites had high concentrations of Eagle Pass Tracer more often due to a much greater frequency of transport to them. These sites were also more likely to be near the center of the tracer concentration distribution than near the edge, as would occur often for the sites to the south. During the latter half of the study (September-October), the north-south gradient in tracer was reduced. Averaged over all 6-hour sites, the ocPDCH concentrations were about 1/3 lower during the 2 pm-8 pm CDT monitoring period compared to the three other periods; it seems probable that these lower concentrations are due to enhanced mixing at this time if day.

Time series plots of the influence functions for the continuously released tracers are shown in Figures 5-19 through 5-22. Note that the vertical scales differ from figure to figure.

The Eagle Pass tracer often has elevated concentrations at one or more sites, although at the two southernmost sites Big Bend and San Vicente, concentrations are often near baseline. For the other three release sites, maximum influence functions are about an order of magnitude lower than for the Eagle Pass release, reflecting their greater distance and correspondingly greater dispersion. Elevated concentrations are also much less frequent for these release locations as well.

Northeast Texas tracer concentrations were near background much of the time with a few exceptions when they were significantly above background at multiple 6-hour sampling sites. Such behavior was particularly notable during an August 20-22 high particulate matter concentration episode and during October 23 to 26. Note that the Northeast Texas tracer was not released between October 8 and 16.

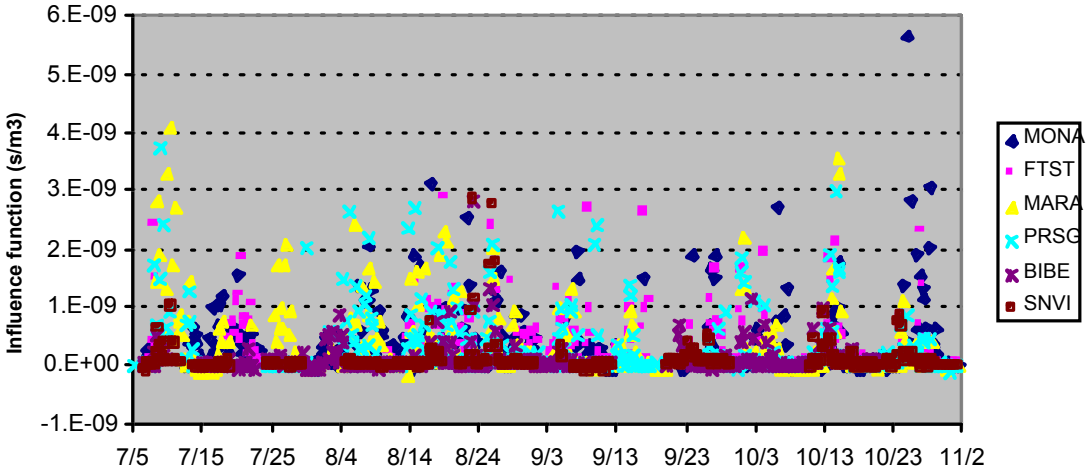

Figure 5-19. *Time series of influence functions at 6-hr sampling sites for the Eagle Pass continuous tracer, ocPDCH.*

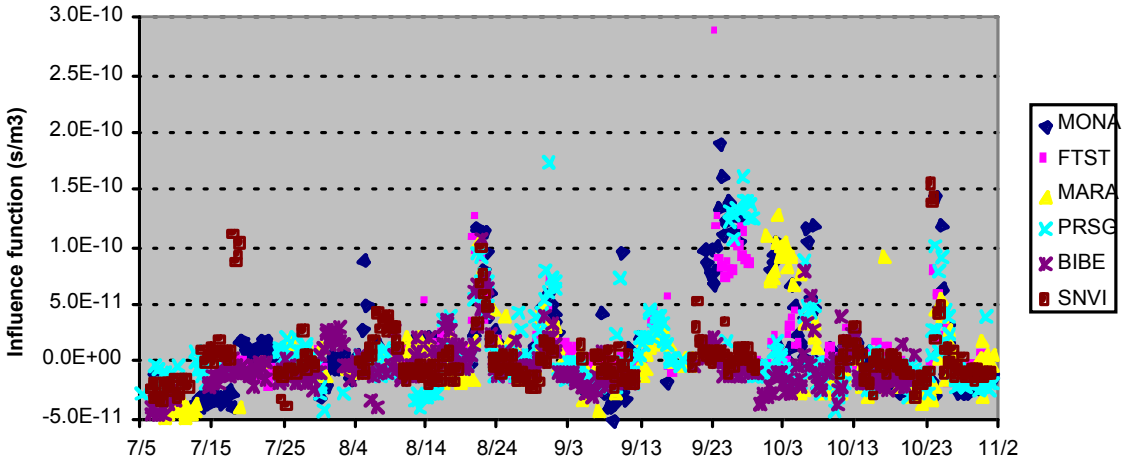

Figure 5-20. *Time series of influence functions at 6-hr sampling sites for the Northeast Texas tracer, i-PPCH.*

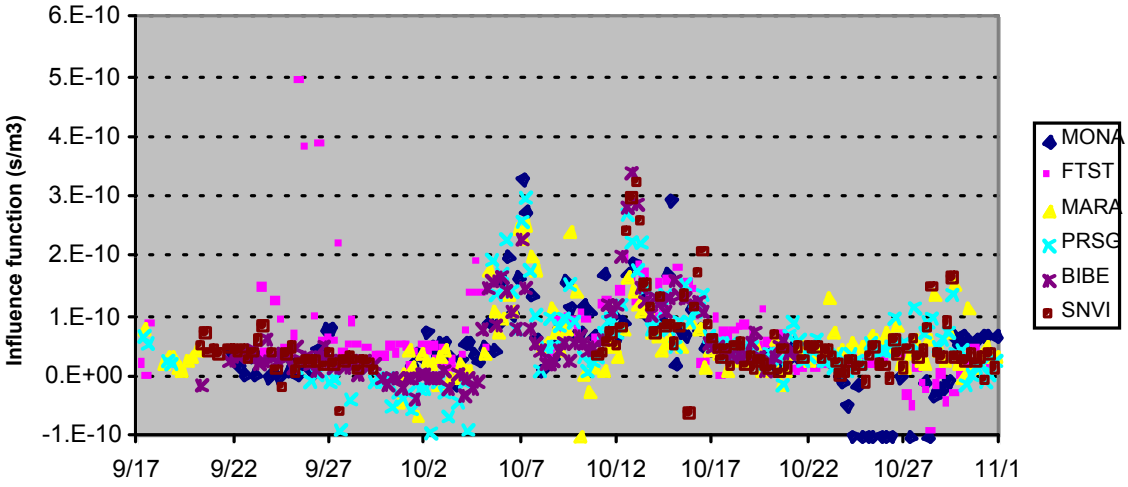

***Figure 5-21**. Time series of influence functions at 6-hr sampling sites for the San Antonio tracer, PDCB.*

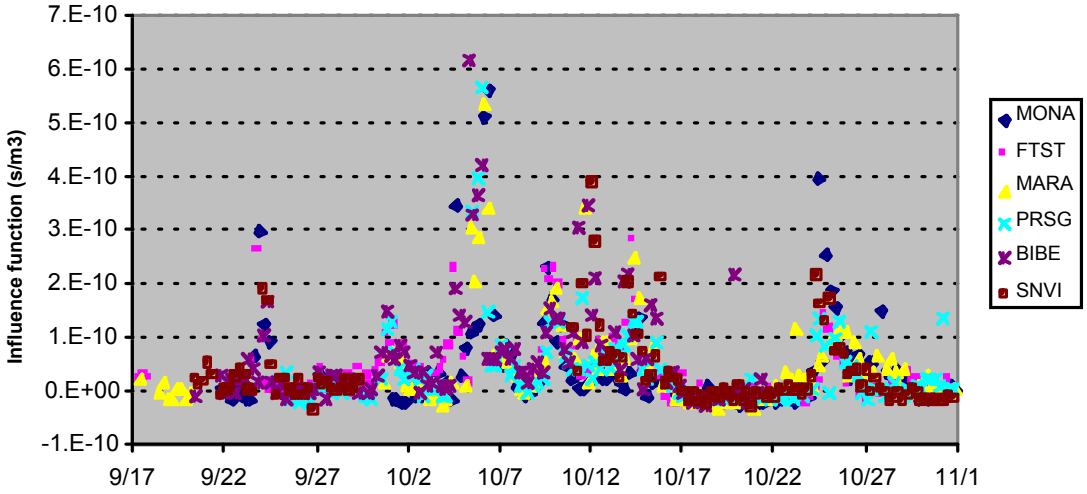

***Figure 5-22**. Time series of influence functions at 6-hr sampling sites for the Houston tracer, PTCH.*

The San Antonio tracer showed elevated concentrations at all 6-hour site for two main periods, October 5-8, and October 11-16. Both of these periods corresponded at to high sulfate concentrations for some of the days. A smaller, broader peak was evident at some sites in late October.

The tracer released from Houston showed elevated levels at all sites for much of the periods October 4-7, October 9-15, and October 24-26. The first two of these periods corresponded to periods of high sulfate concentrations.

5.5.2 Analysis of Timing Tracer Data

As described in Section 3.2, during the first portion of the study (5 July to 13 September 1999) three tracers were released from a tower at Eagle Pass: ocPDCH was released continuously; PDCB was released on alternate days (8am CDT to 8 am CDT); and PTCH was released 8 am to 8 pm CDT, corresponding with the diurnal period of expected well-mixed conditions. By comparing the ratios of tracer concentrations in a sample, we can obtain information regarding the sample's fraction of the continuously-released tracer that was released during daytime versus nighttime conditions. We can also obtain a range of transport times corresponding to each sample.

The influence functions for the alternate day tracer PDCB are plotted against the influence function for the continuous tracer ocPDCH at the 6-hour sites in Figure 5-23. If the continuous tracer measured for a particular sample was released during the period that the alternate day tracer was being released, the influence functions should be equal for the two tracers. Conversely if the sampled continuous tracer was released during a period of no release of the alternate day tracer, the alternate day tracer concentration (above background) should be zero. Thus the ratio of alternate day tracer to continuous tracer should range from zero to one.

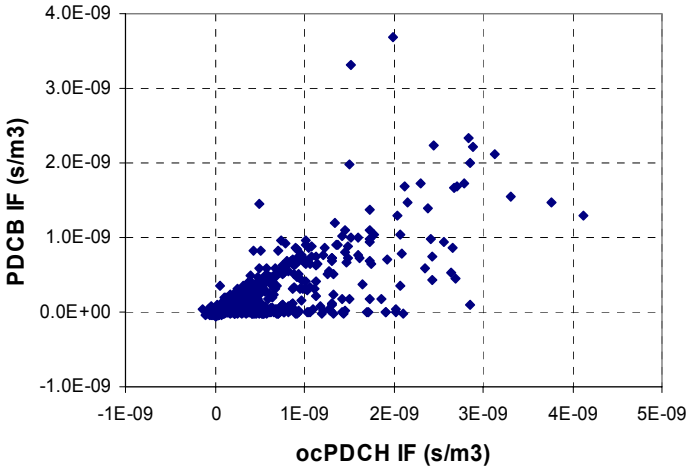

Figure 5-23. *Alternate day tracer PDCB versus continuous tracer ocPDCH influence functions at 6 hour sites for periods of timing tracer release (7/5/99- 9/13/99).*

Note that, excluding a few outlying data points, there is an upper bound line that corresponds to approximately equal influence functions for each tracer. Data strongly suggest that these samples corresponded to periods where both tracers were being released. Another group of data lies along a line with significant influence functions from the continuous tracer, but essentially zero above-background concentration of the every other day tracer. These data points should correspond to tracer releases during the days in which the alternate day tracer was shut off. Data points in-between the zero and 1:1 line correspond to periods in which the alternate day tracer was released for a portion of the release period being sampled.

Figure 5-24 is a similar plot that compares the daytime only (8 am – 8 pm CDT) tracer PTCH to the continuous tracer ocPDCH at the six hour sampling sites. Again, with a few outliers, there is a distinct upper limit at a ratio of 1:1, corresponding to daytime periods where both tracers were being released and a lower line corresponding to nighttime release periods. Data between the zero and 1:1 line correspond to release periods including both daytime and nighttime hours.

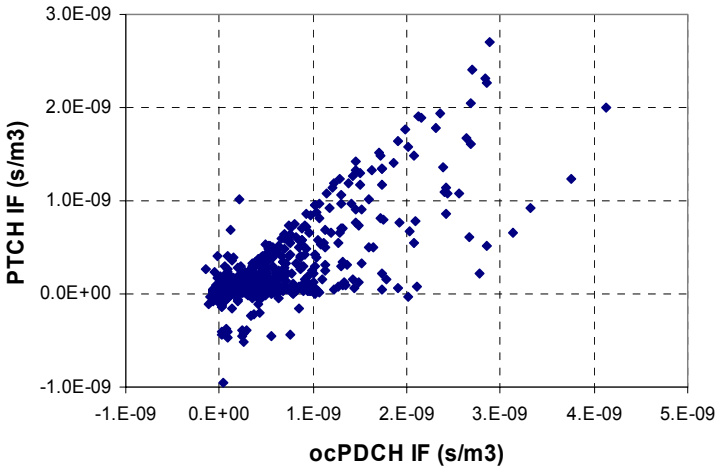

Figure 5-24. *Daytime only (8 am to 8 pm CDT) tracer PTCH versus continuous tracer ocPDCH influence functions at 6 hour sites for periods of timing tracer release (7/5/99- 9/13/99).*

The timing tracers also offer information concerning the speed with which emissions from Eagle Pass are advected downwind and diffused along the wind. The full extraction and interpretation of this information requires detailed analyses employing three-dimensional transport models. Some indication of the success of this effort can, however, be gained directly from the tracer data themselves.

Viewed individually, the different tracers concentrations vary greatly from sample to sample, in response to atmospheric changes that even the most advanced models have difficulty accounting for. However, the timing (PDCB, PTCH) and marking (ocPDCH) tracers released into a given air parcel experience exactly the same sequence of atmospheric processing, and their relative abundance is therefore unaffected. The tracer concentration ratios PDCB/ocPDCH and PTCH/ocPDCH thus retain information on when the sampled material was released: on an even or odd day, in daytime or nighttime, or some combination produced by mixing parcels of differing ages.

Figure 5-25 shows these timing signals to have been evident at monitors over 300 km downwind of Eagle Pass. Because the signals repeat every 48 hours, and our wind data yield predicted transport times generally shorter than this, times are plotted for repeating 48-hour periods with PDCB released for the first 24 hours of each period. This data plotting method highlights the observed periodicity of the ambient concentrations.

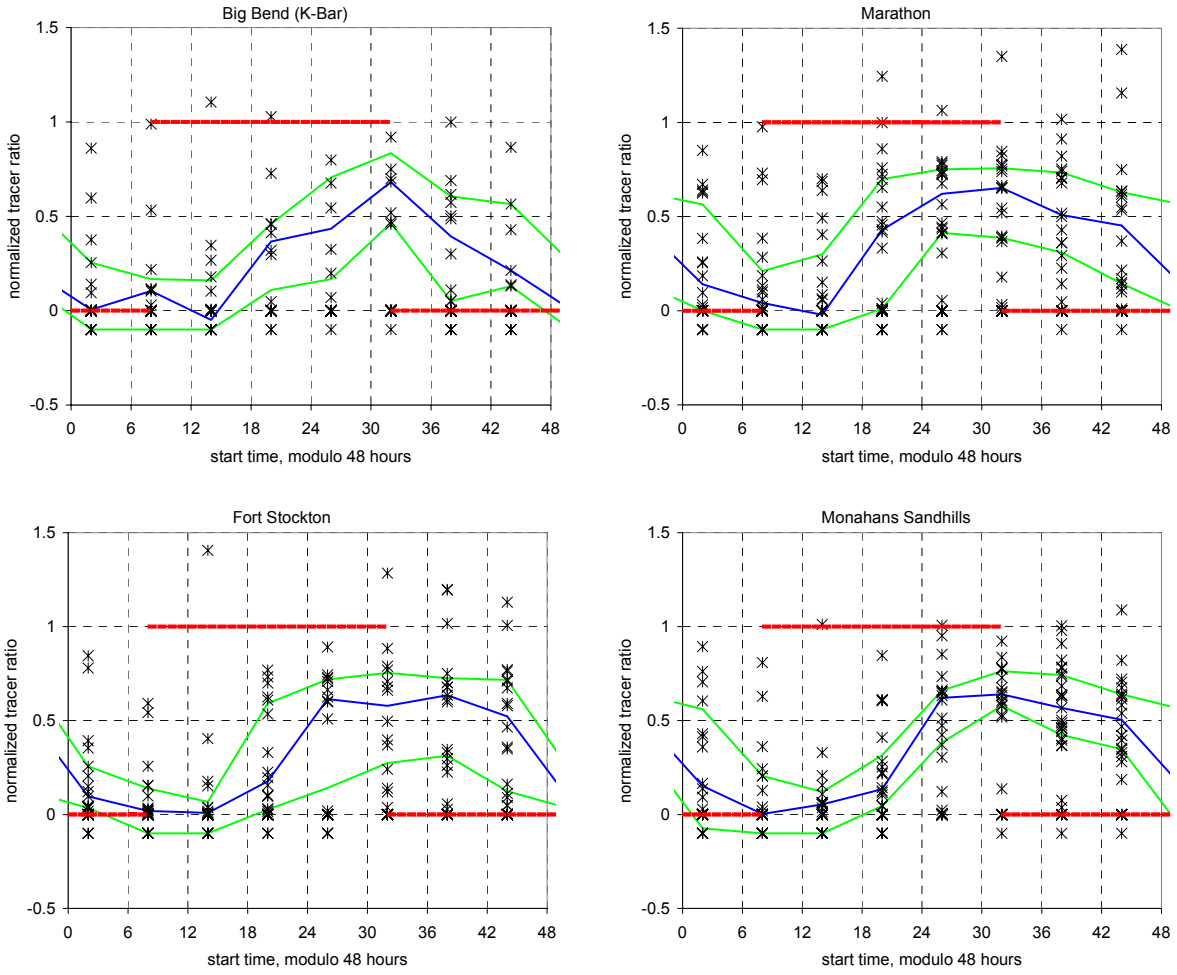

Figure 5-25. *Normalized ratio of PDCB to ocPDCH released from Eagle Pass at four monitoring sites. PDCB was released on alternate days. The blue and green lines join the median and quartile values in each 6-hour interval.*

The ocPDCH tracer was released continuously from Eagle Pass from 5 July to 13 September, accompanied by 24-hour releases of PDCB on alternate days as indicated by the red horizontal lines. In Figure 5-25, symbols show the above-background-concentration ratios of PDCB to ocPDCH in individual 6-hour ambient samples. The ambient ratios are normalized to the nominal ratio in the release rates, and are plotted only for observations in which ocPDCH was in the upper two-thirds of the values observed at all four sites over the entire period. Ratios arising from negative PDCB values are plotted at –0.1. There is scatter in the ratios because the data points represent two months of measurements in a range of synoptic flow conditions, and thus reflect different transport times. The blue and green curves join the median and quartile values in each 6-hour interval.

Figure 5-25 shows a 48-hour pattern in the ocPDCH to PDCB ratio. The differences between the ratio quartile values demonstrate typical variability in transport conditions, especially transport speed.

The same analysis (not shown here) was also carried out for the daytime tracer PTCH and its results are consistent with the ones shown here.

A method of directly estimating transport times was to assign each ambient sample to one of four 12-hour release periods in each 48-hour period whenever the continuous tracer was significantly above background (more than twice the uncertainty above background). This was done by using both the alternate day and daytime tracers, in which case each 12-hour period has a unique combination of tracers being released, and assuming a transport time of less than 48 hours. Using this method, the percentages of estimated transport times for each 6-hour range, averaged over all sites, are shown in Figure 5-26. The peak of the estimated transport time distribution is at 15 hours, which corresponds to transport speeds of about 5-6 m/s, depending upon the distance to the monitoring site.

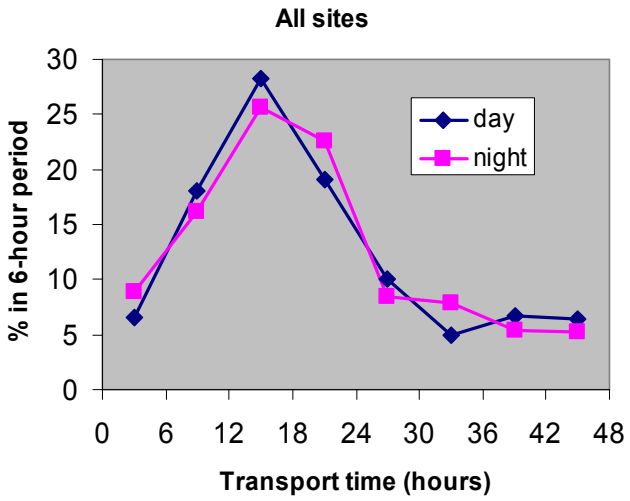

Figure 5-26. *Distribution of estimated transport times of Eagle Pass tracers to 6-hour monitoring sites in each 6-hour period during the timing tracer study (7/5/99-9/13/99). Percentages are averaged over all 6-hour sampling sites separately for daytime and nighttime releases.*